JAERI-M
7287

HEAT FLUX IN THE DIVERTOR REGION OF DIVA

September 1977

Haruyuki KIMURA, Noriaki UEDA*, Hikosuke MAEDA
Shin YAMAMOTO, Masayuki NAGAMI, Kazuo ODAJIMA
Seio SENGOKU, Yasuo SHIMOMURA, Masahiro SEKI
and Hiroshi KAWAMURA

日本原子力研究所
Japan Atomic Energy Research Institute

この報告書は，日本原子力研究所がJAERI-Mレポートとして，不定期に刊行している研究報告書です．入手，複製などのお問合わせは，日本原子力研究所技術情報部（茨城県那珂郡東海村）あて，お申しこしください．

JAERI-M reports, issued irregularly, describe the results of research works carried out in JAERI. Inquiries about the availability of reports and their reproduction should be addressed to Division of Technical Information, Japan Atomic Energy Research Institute, Tokai-mura, Naka-gun, Ibaraki-ken, Japan.

JAERI-M 7287

Heat Flux in the Divertor Region of DIVA

Haruyuki KIMURA, Noriaki UEDA*, Hikosuke MAEDA, Shin YAMAMOTO, Masayuki NAGAMI, Kazuo ODAJIMA, Seio SENGOKU, Yasuo SHIMOMURA, Masahiro SEKI+, and Hiroshi KAWAMURA+

Division of Thermonuclear Fusion Research, Tokai Research Establishment, JAERI

(Received August 24,1977)

Time and spatially resolved measurements of heat and particle fluxes in the divertor of DIVA were made. On the electron side of the divertor, relatively large heat flux exists even in the absence of runaway electrons. This large heat flux possibly causes the plasma contamination by heavy impurities in DIVA. By detailed measurements,it is concluded that this large heat flux is due to the epithermal electrons in the energy range from 100 to 200 eV. A quantitative relationship is obtained between the heat and the particle flux; which is well explained by a simple sheath model including the effect of epithermal electrons.

Keywords: DIVA Tokamak, Heat Flux, Particle Flux, Runaway Electron, Heavy Impurity, Sheath Model

---

* Present address Mitsubishi Atomic Power Industry, Saitama, Japan

+ Division of Reactor Engineering, Tokai Research Establishment, JAERI

DIVAのダイバーター領域における熱流束

日本原子力研究所東海研究所核融合研究部
木村　晴行・上田　憲照*・前田　彦祐
山本　新・永見　正幸・小田島　和夫
仙石　盛夫・下村　安夫・関　昌弘+・
河村　洋+

（1977年8月24日受理）

DIVAのダイバーター領域における熱流束・粒子束に対して時間的・空間的分解能の良い測定が行なわれた。ダイバーター部で電子がトロイダル電界によって加速される側では逃走電子が存在しない場合にでも比較的大きな熱流束が存在する。DIVAに於ける金属不純物はこの比較的大きな熱流束に依ると考えられている。詳細な測定の結果，この熱流束はエネルギー領域が100から200電子ボルト程度の比較的低エネルギーの電子に依ることが結論される。熱流束と粒子束との間の量的な関係が得られ，且つこれが上述の電子の効果を入れた簡単なシースモデルで良く説明できる。

＊　外来研究員三菱原子力工業株式会社
＋　日本原子力研究所東海研究所原子炉工学部

Contents

1. Introduction

Recently, Impurity study has been one of the main subjects in tokamak research. In DIVA [1-5], a tokamak with an axisymmetric poloidal divertor, an intensive investigation about this matter has been performed.

In Ref. [1] it is concluded that not light but heavy impurities are influential in DIVA and responsible for the radiation loss from the main plasma. It is also described in Ref. [1] that heat flux to the divertor is a possible cause of the plasma contamination by evaporation of the structural materials. So that in this sense, the reduction of heat flux to the divertor must be indispensable, especially for a next-generation divertor tokamak. To this end it is important to obtain scaling law of heat flux to the divertor by the present-day divertor tokamak.

It is well known that a sheath potential built up in front of an electrically insulated conducting plate plays an important role for a thermal barrier. Heat flux q (Watts/cm^2) to an electrically insulated conducting plate in a plasma is written as follows [6].

$$q = \gamma I_s \cdot T_e \qquad (1)$$

where I_s(A/cm^2) is ion saturation current density, T_e(eV) is electron temperature and γ is called as a heat transmission rate, and $\gamma = 7.8$ for hydrogen plasma of $T_e = T_i$, where T_i is proton temperature. As noted in previous experiments [3, 5], heat fluxes in the divertor are highly asymmetric as to the median plane and high energy electrons escaping from the main plasma cause this asymmetry, since they can exist in one side of the divertor until they annihilate at the neutralizer plate. Hereafter we distinguish each side of the divertor as to the median plane as an electron side and ion side of divertor, respectively. In the electron side, γ is a few to ten times larger than the value estimated by Eq.(1). Moreover even in the case with an additional hydrogen gas injection after starting a discharge, γ is a few times larger than expected, although the amount of high energy electrons is considerable reduced. However above experiments, more or less, have a lack of accuracy, although in the scrape-off layer of DIVA various types of probes has been successfully used [7]. The thermocouple used at first for a heat flux measurement has a response time of 5 ms, which is too large for our experiment, since in this time interval ion saturation current and electron temperature change considerably. In addition, the use of a Langmuir probe for the measurement of I_s and T_e may be difficult particularly in the presence of high energy electrons.

This time we have developed a thin - film thermometer [8-9] with a response time 0.2 ms, which is small enough for our experiment. As for a particle measurement, an electrostatic multigrid energy analyzer is used, which is able to measure I_s and T_e even in the presence of high energy electrons.

With these powerful tools we have had a detailed knowledge about heat and particles in the divertor. In this paper we make a relationship between heat and particle fluxes in the divertor clear.

2. Thermometer and Multi-grid Energy Analyzer

The detailed description of the thin - film thermometer is given elsewhere [8-9]. Here some brief description is pressented. Fig.1 shows structure of the thermometer. A backing metal was a thin molybdenum plate of 8×12 mm^2 area and 0.1 mm thickness. Silicon monoxide was deposited in vacuum on the molybdenum plate and then nickel on it. The silicon monoxide layer served as an electrical insulator. Temperature of the molybdenum was measured by resistance change of the nickel film. The response time of the thermometer was measured using Q switch pulse laser and was found less than 0.2 ms.

The width of the nickel film is 0.4 mm which is much larger than the thickness of the molybdenum plate. So that a spatial resolution of the thermometer is determined by the width of the nickel film.

Fig.2 shows the multigrid energy analyzer schematically. The external jacket of the analyzer is at the same potential as the vacuum vessel. In front of stainless steel collector plate C, 5 mm in diameter, three stainless steel grids (E, G_1, G_2) are placed with the distance of 1 mm. The grid E with the same potential as the vacuum vessel has eight channels, 100 μm in diameter and 100 μm long, in 1 mm aperture, which decides a spatial resolution of this analyzer. The mesh grids G_1 and G_2 are of 20 and 50 μm wires and have a transparency of 0.31 and 0.44, respectively.

Fig.3 shows potential distributions between three grids and a collector plate to obtain ion and electron velocity distributions. Ion saturation currents are obtained by the following procedure, even in the presence of high energy electrons and freely from a secondary electron emission effect. That is, we adopt the potential profile shown in Fig.3 (a) and subtract the collector signal at +150 V from one at -40 V. The latter composes of ion saturation current plus electron leakage current, while the former composes of electron leakage current only, which must be equal regardless of a collector potential.

This time we have developed a thin - film thermometer [8-9] with a response time 0.2 ms, which is small enough for our experiment. As for a particle measurement, an electrostatic multigrid energy analyzer is used, which is able to measure I_s and T_e even in the presence of high energy electrons.

With these powerful tools we have had a detailed knowledge about heat and particles in the divertor. In this paper we make a relationship between heat and particle fluxes in the divertor clear.

2. Thermometer and Multi-grid Energy Analyzer

The detailed description of the thin - film thermometer is given elsewhere [8-9]. Here some brief description is pressented. Fig.1 shows structure of the thermometer. A backing metal was a thin molybdenum plate of 8 × 12 mm² area and 0.1 mm thickness. Silicon monoxide was deposited in vacuum on the molybdenum plate and then nickel on it. The silicon monoxide layer served as an electrical insulator. Temperature of the molybdenum was measured by resistance change of the nickel film. The response time of the thermometer was measured using Q switch pulse laser and was found less than 0.2 ms.

The width of the nickel film is 0.4 mm which is much larger than the thickness of the molybdenum plate. So that a spatial resolution of the thermometer is determined by the width of the nickel film.

Fig.2 shows the multigrid energy analyzer schematically. The external jacket of the analyzer is at the same potential as the vacuum vessel. In front of stainless steel collector plate C, 5 mm in diameter, three stainless steel grids (E, G_1, G_2) are placed with the distance of 1 mm. The grid E with the same potential as the vacuum vessel has eight channels, 100 μm in diameter and 100 μm long, in 1 mm aperture, which decides a spatial resolution of this analyzer. The mesh grids G_1 and G_2 are of 20 and 50 μm wires and have a transparency of 0.31 and 0.44, respectively.

Fig.3 shows potential distributions between three grids and a collector plate to obtain ion and electron velocity distributions. Ion saturation currents are obtained by the following procedure, even in the presence of high energy electrons and freely from a secondary electron emission effect. That is, we adopt the potential profile shown in Fig.3 (a) and subtract the collector signal at +150 V from one at -40 V. The latter composes of ion saturation current plus electron leakage current, while the former composes of electron leakage current only, which must be equal regardless of a collector potential.

3. Experimental Procedure and Results

Fig.4 shows cross-sectional view of DIVA. The experiment was performed under the following operational conditions. The toroidal magnetic field is fixed at 1 T. Ratio of a divertor hoop current to a plasma current is 1.2, where the latter is 14 kA at a flattop. The base pressure is 1×10^{-7} torr, and hydrogen gas of 1.5×10^{18} atoms was admitted by four fast - acting valves 0.8 ms before starting a discharge. An additional hydrogen gas was injected 2.2 ms after starting a discharge at a rate of 1.7×10^{19} H_2/S.

Central electron and ion temperature were 200 and 80 eV from laser scattering and charge exchange neutrals, respectively. Average electron density was 1×10^{13} cm^{-3} from 4 mm μ-wave interferometer.

A thermometer and a multigrid analyzer were scanned along the toroidal azis at R = 40 cm.

Fig.5 shows typical thermometer data. This figure represents resistance change of Ni thin-film. The temperature T of the thin-film, which is assumed to be equal to that of the molybdenum plate, is obtained from a calibration curve. If heat flux to the divertor has a very sharp peak in space, we must take heat conduction in the molybdenum plate into account to calculate heat flux from the measured temperature [9]. In the present paper, however, heat flux is calculated from a simple heat balance equation.

$$q(z, t) = \rho c d \frac{dT(z, t)}{dt} \qquad (2)$$

where ρ, c, and d are density, specific heat and thickness of the molybdenum backing plate, respectively. Fig.6 shows Z-profile of heat flux in the electron side of the divertor. This profile indicates a sharp peak at z=45 mm. This fact seems to be inconsistent with the preceding context. However, even if heat conduction in the molybdenum plate is taken into account, the peak value of the heat flux profile increaces at most factor of 1.5. Next, we describe the results of particle measurements.

Fig.7 shows time variation of electron energy spectra at z=45 mm. These spectra were obtained changing the bias voltage of grid G_2 of the multigrid analyzer shot by shot. It was turned out that relatively high energy electrons, whose energy range is 100 to 200 eV, exist in a narrow layer in the electron side of divertor, i.e. z=45 $\sim$ 50 mm and that the amount of these electrons varies with time. In order to examine much higher range of energy than that of the multigrid analyzer, we scanned X-ray target [10], whose spatial resolution is 1 mm, in the electron side

of divertor. X-ray energy observed with 100% efficiency ranges approximately from 10 to 100 keV determined by the thickness of Aluminum window and the height of an NaI scintillator. Fig.8 shows Z-profile of X-ray intensity I_x from the target. The profile of electron flux whose energy is larger than 150 eV is also depicted in this figure. The peak position of I_x is 42.5 mm, where heat flux is much smaller than that of z=45.0 mm.

The measurement of ion saturation current density was also made by the procedure described in the previous section. Ion saturation current density and bulk temperature of electrons are shown in Fig.6. It is noted here that measured heat flux is factor $2 \sim 3$ larger than the values calculated from Eq.(1) using measured ion saturation current density and bulk temperature of electrons.

4. Discussions

It is natural that this relatively large heat flux is due to the electrons in 100-200 eV range of energy. Hereafter we call those as epithermal electrons. The loss mechanism of the epithermal electrons from the main plasma column is discussed in Ref.[10]. To confirm above matter we make some simple analysis following to Lovberg [6]. We assume electron velocity distribution as a two component Maxwellian. That is,

$$n_e = \sum_{k=1}^{2} n_{ek} \left(\frac{m}{2\pi T_{ek}}\right)^{\frac{1}{2}} \exp\left(-\frac{mv_\parallel^2}{2T_{ek}}\right) \qquad (3)$$

where n_e and m are the density and mass of electrons and suffixes 1 and 2 refer to low and high energy components, respectively. Furthermore we make two assumptions. 1) ion temperature T_i is equal to T_{e1}. This fact was roughly assured in the scrape-off layer by a multi-grid analyzer. 2) No secondary electron is emitted from a backing plate of a thermometer.

A floating potential ϕ_o of a backing plate, where a space potential is set to be zero, can be determined by the condition that net current to this plate is equal to be zero. That is,

$$\sum_{k=1}^{2} \frac{1}{4} n_{ek} \left(\frac{8T_{ek}}{\pi m}\right)^{\frac{1}{2}} \exp\frac{e\phi_o}{T_{ek}} = \frac{\xi}{4} n_o \left(\frac{8T_i}{\pi M}\right)^{\frac{1}{2}} \qquad (4)$$

where n_o is ion density, M is ion mass and ξ is a correction factor of electron to ion saturation current ratio in a strong magnetic field.

Calculated ϕ_o from Eq.(4) using ξ=4 and experimental data of T_{e1}, T_{e2} and n_{e2}/n_{e1} is in good agreement with experiment. Fig.8 shows comparison between measurements with spatial resolution 0.3 mm and calculation of ϕ_o,

of divertor. X-ray energy observed with 100% efficiency ranges approximately from 10 to 100 keV determined by the thickness of Aluminum window and the height of an NaI scintillator. Fig.8 shows Z-profile of X-ray intensity I_x from the target. The profile of electron flux whose energy is larger than 150 eV is also depicted in this figure. The peak position of I_x is 42.5 mm, where heat flux is much smaller than that of z=45.0 mm.

The measurement of ion saturation current density was also made by the procedure described in the previous section. Ion saturation current density and bulk temperature of electrons are shown in Fig.6. It is noted here that measured heat flux is factor 2 ~ 3 larger than the values calculated from Eq.(1) using measured ion saturation current density and bulk temperature of electrons.

4. Discussions

It is natural that this relatively large heat flux is due to the electrons in 100-200 eV range of energy. Hereafter we call those as epithermal electrons. The loss mechanism of the epithermal electrons from the main plasma column is discussed in Ref.[10]. To confirm above matter we make some simple analysis following to Lovberg [6]. We assume electron velocity distribution as a two component Maxwellian. That is,

$$n_e = \sum_{k=1}^{2} n_{ek}\left(\frac{m}{2\pi T_{ek}}\right)^{\frac{1}{2}} \exp\left(-\frac{mv_o^2}{2T_{ek}}\right) \qquad (3)$$

where n_e and m are the density and mass of electrons and suffixes 1 and 2 refer to low and high energy components, respectively. Furthermore we make two assumptions. 1) ion temperature T_i is equal to T_{e1}. This fact was roughly assured in the scrape-off layer by a multi-grid analyzer. 2) No secondary electron is emitted from a backing plate of a thermometer.

A floating potential ϕ_o of a backing plate, where a space potential is set to be zero, can be determined by the condition that net current to this plate is equal to be zero. That is,

$$\sum_{k=1}^{2} \frac{1}{4} n_{ek}\left(\frac{8T_{ek}}{\pi m}\right)^{\frac{1}{2}} \exp\frac{e\phi_o}{T_{ek}} = \frac{\xi}{4} n_o\left(\frac{8T_i}{\pi M}\right)^{\frac{1}{2}} \qquad (4)$$

where n_o is ion density, M is ion mass and ξ is a correction factor of electron to ion saturation current ratio in a strong magnetic field.

Calculated ϕ_o from Eq.(4) using ξ=4 and experimental data of T_{e1}, T_{e2} and n_{e2}/n_{e1} is in good agreement with experiment. Fig.8 shows comparison between measurements with spatial resolution 0.3 mm and calculation of ϕ_o,

where the potential of vacuum chamber was set to be zero and the space potential was equal to about 20 V with respect to the vacuum chamber, that was assured by a Langmuir probe. Heat flux to a thermometer is written as

$$q = I_s \cdot T_{el} \left(\frac{2}{\xi} \cdot \sqrt{\frac{M}{m}} \left\{(1-\varepsilon) \exp\frac{e\phi_o}{T_{el}} + \varepsilon h \exp\frac{e\phi_o}{T_{e2}}\right\} + 2 - \frac{e\phi_o}{T_{el}}\right) \quad (5)$$

where $h = T_{e2}/T_{el}$ and $\varepsilon = \frac{n_{e2}}{n_o}$.

This may be compared with heat flux in the absence of high energy tail, by rewriting in the form

$$q = F \cdot \gamma \cdot I_s \cdot T_{el} \quad (6)$$

where γ is a heat transmission rate in the absence of high energy tail, equal to 6.4 for hydrogen plasm and $\xi=4$, and F is a correction factor for a two component model.

If the high energy term in the left side of Eq.(4) is dominant, F is approximately written as follows.

$$F = \frac{1}{6.4}\left(2h + 2 - h\ell n \frac{\varepsilon\sqrt{\frac{m}{M}}}{\varepsilon\sqrt{h}}\right) \quad (7)$$

This approximate form of F is in agreement with the exact value from Eq.(5) within 10% using the measured values of h and ε.

Fig. 9 shows a relationship between heat flux q measured in the electron side of divertor and correction factor F calculated exactly from Eq.(4-5) using experimental data of h and ε. The values of q corresponding to F=1 are those in the absence of epithermal electrons. It is elucidated that strong correlation between the relatively large heat flux and the existence of epithermal electrons. However measured q is not necessarily in good agreement with $F\gamma I_s T_{el}$. In some cases q is factor of 2 larger than $F\gamma I_s T_{ei}$. One of the possible explanation for this discrepancy is that a floating potential of a backing plate of a thermometer is shallower than expected from Eq.(4), since the dimension of a backing plate, 8 mm, is larger than characteristic length of a spatial variation of floating potential.

If a bias voltage of a thermometer is shallower than a local folating potential, larger heat flux is gained than that of a local floating plate. In order to confirm this subject, the dependence of heat flux on the bias voltage of a sheath of a thermocoaxis whose diameter is 0.25 mm was examined. Fig.10 shows time integrated heat flux to a thermocoaxis as a

function of a bias voltage with respect to a vacuum chamber.

In this figure probe characteristics is also depicted, obtained by employing a sheath of a thermocoaxis as an electrode.

The minimum value of a heat flux is realized in the vicinity of $\phi = \phi_o - \frac{T_e}{e}$, that is consistent with rough calculation. Above this potential, the heat flux increases exponentially.

The other possibility is a secondary electron emission effect, which effect is pointed out in Ref.(11). For the electrons whose energy range is 100 to 200 eV, secondary electron emission rate may not be neglected. In the present experiment the flux of these electrons are not so large that they affect a heat transmission rate considerably, although it is necessary to examine this effect experimentally.

Present experiment was performed under the discharge condition with an additional gas injection. Relatively large heat flux in the electron side of divertor has a strong correlation with epithermal electrons whose energy range is 100 to 200 eV. If the amount of additional gas was increased, the number and kinetic energy of epithermal electrons became small. Hence heat flux was also relatively small.

On the contraty, in the case of no additional gas injection, the heat flux becomes much large and denotes a strong corelation with X-ray intensity i.e. runaway electrons.

Fig.11 shows correlation between time integrated heat flux and time integrated X-ray intensity from a target.

The peak values of heat flux at 15 ms for various discharge conditions are tabulated in Table 1.

5. Conclusion

Heat and particle measurements were performed in the divertor of DIVA in detail. Relatively large heat flux, which is possible cause of plasma contamination in DIVA, exists in the electron side of divertor even with an additional gas injection after starting a discharge. Epithermal electrons whose energy range is 100 to 200 eV are responsible for this large heat flux. Heat flux to the divertor can be reduced with increacing the amount of an additional gas injection.

function of a bias voltage with respect to a vacuum chamber.

In this figure probe characteristics is also depicted, obtained by employing a sheath of a thermocoaxis as an electrode.

The minimum value of a heat flux is realized in the vicinity of $\phi = \phi_o - \frac{T_e}{e}$, that is consistent with rough calculation. Above this potential, the heat flux increases exponentially.

The other possibility is a secondary electron emission effect, which effect is pointed out in Ref.(11). For the electrons whose energy range is 100 to 200 eV, secondary electron emission rate may not be neglected. In the present experiment the flux of these electrons are not so large that they affect a heat transmission rate considerably, although it is necessary to examine this effect experimentally.

Present experiment was performed under the discharge condition with an additional gas injection. Relatively large heat flux in the electron side of divertor has a strong correlation with epithermal electrons whose energy range is 100 to 200 eV. If the amount of additional gas was increased, the number and kinetic energy of epithermal electrons became small. Hence heat flux was also relatively small.

On the contraty, in the case of no additional gas injection, the heat flux becomes much large and denotes a strong corelation with X-ray intensity i.e. runaway electrons.

Fig.11 shows correlation between time integrated heat flux and time integrated X-ray intensity from a target.

The peak values of heat flux at 15 ms for various discharge conditions are tabulated in Table 1.

5. Conclusion

Heat and particle measurements were performed in the divertor of DIVA in detail. Relatively large heat flux, which is possible cause of plasma contamination in DIVA, exists in the electron side of divertor even with an additional gas injection after starting a discharge. Epithermal electrons whose energy range is 100 to 200 eV are responsible for this large heat flux. Heat flux to the divertor can be reduced with increacing the amount of an additional gas injection.

Acknowledgement

We are grateful to the Diagnostic Group and the JFT-2a Opration Group f for their help. We should also like to express our gratitude to Drs.M.Tanaka, Y.tanaka, M.Yoshikawa, and S.Mori for their continuing encouragement in this work.

References

(1) MAEDA, H., et al., Proc. Int. Symp. on Plasma Wall Interaction, Jülich, Germany, (1976) 537.

(2) MAEDA, H., et al., 6th Conf. on Plasma Physics and Controlled Nuclear Fusion Research, Berchtesgaden 1976, paper IAEA-CN-35/A-18.

(3) SHIMOMURA, Y., et al., Proc. 7th Europ. Conf. on Controlled Fusion and Plasma Physics, Lausanne, 2 (1975) 81.

(4) SHIMOMURA, Y., et al., Phys. Fluids 19 (1976) 1635.

(5) MAEDA, H., et al., Nucl. Fusion 16 (1976) 148.

(6) LOVBERG, R. H., "Plasma Diagnostic Techniques" (R. H. Huddlestone and S. L. Leonard, ed.) Chap. 3 Academic Press New York (1965).

(7) KIMURA, H., et al., JAPAN ATOMIC ENERGY RESEARCH INSTITUTE REPORT, JAERI-M 6971 (1977).

(8) UEDA, N., et al., JAPAN ATOMIC ENERGY RESEARCH INSTITUTE REPORT, JAERI-M 6723 (1976).

(9) SEKI. M., et al., J. of Nuclear Science and Technology 14 (1977) 534.

(10) YAMAMOTO, S., et al., submitted to Nucl. Fusion.

(11) HOBBS, G. D., and WESSON, J. A., Plasma Physics 9 (1967) 85.

Acknowledgement

We are grateful to the Diagnostic Group and the JFT-2a Opration Group f for their help. We should also like to express our gratitude to Drs.M.Tanaka, Y.tanaka, M.Yoshikawa, and S.Mori for their continuing encouragement in this work.

References

(1) MAEDA, H., et al., Proc. Int. Symp. on Plasma Wall Interaction, Jülich, Germany, (1976) 537.

(2) MAEDA, H., et al., 6th Conf. on Plasma Physics and Controlled Nuclear Fusion Research, Berchtesgaden 1976, paper IAEA-CN-35/A-18.

(3) SHIMOMURA, Y., et al., Proc. 7th Europ. Conf. on Controlled Fusion and Plasma Physics, Lausanne, 2 (1975) 81.

(4) SHIMOMURA, Y., et al., Phys. Fluids 19 (1976) 1635.

(5) MAEDA, H., et al., Nucl. Fusion 16 (1976) 148.

(6) LOVBERG, R. H., "Plasma Diagnostic Techniques" (R. H. Huddlestone and S. L. Leonard, ed.) Chap. 3 Academic Press New York (1965).

(7) KIMURA, H., et al., JAPAN ATOMIC ENERGY RESEARCH INSTITUTE REPORT, JAERI-M 6971 (1977).

(8) UEDA, N., et al., JAPAN ATOMIC ENERGY RESEARCH INSTITUTE REPORT, JAERI-M 6723 (1976).

(9) SEKI. M., et al., J. of Nuclear Science and Technology 14 (1977) 534.

(10) YAMAMOTO, S., et al., submitted to Nucl. Fusion.

(11) HOBBS, G. D., and WESSON, J. A., Plasma Physics 9 (1967) 85.

Table 1 Comparison between peak values of heat flux for different discharge conditions.

Rate of an additional gas injection	Peak values of heat flux
0 H_2/s	2200 Watts/cm^2
4.5×10^{19}	430
1.7×10^{19}	180

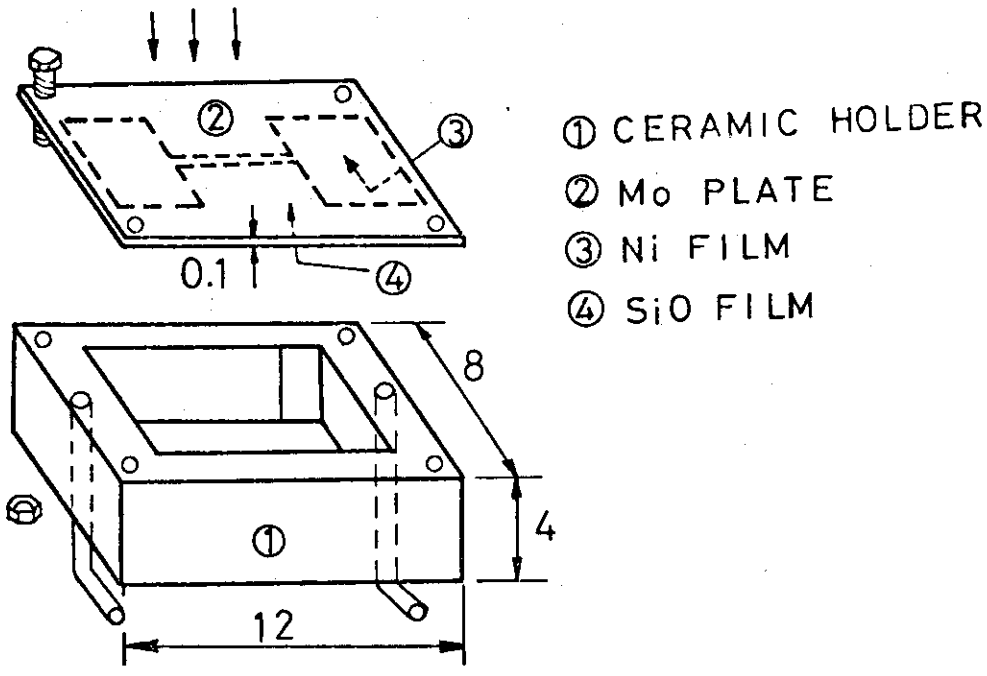

Fig. 1 Schematic drawing of a thermometer.

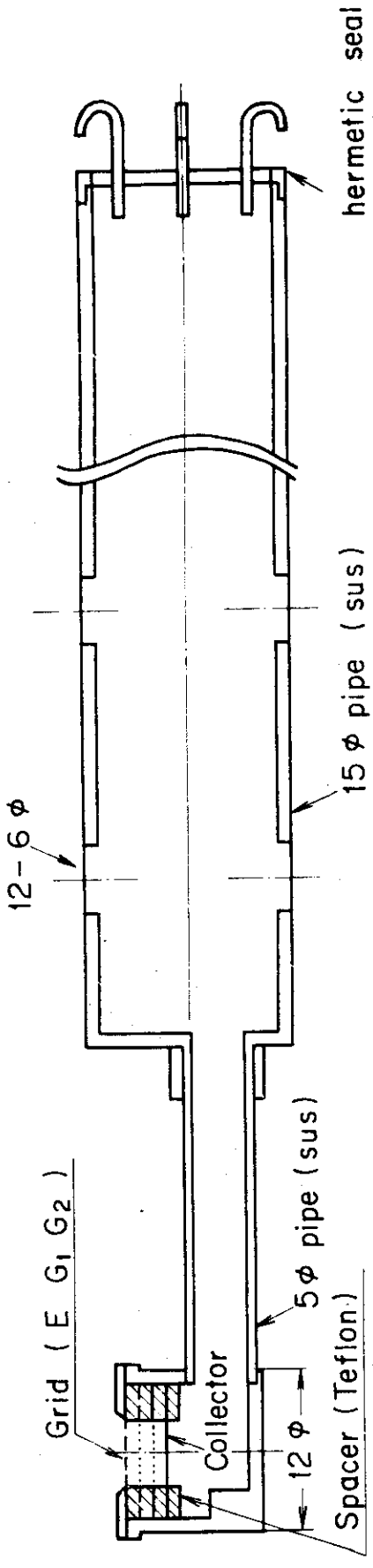

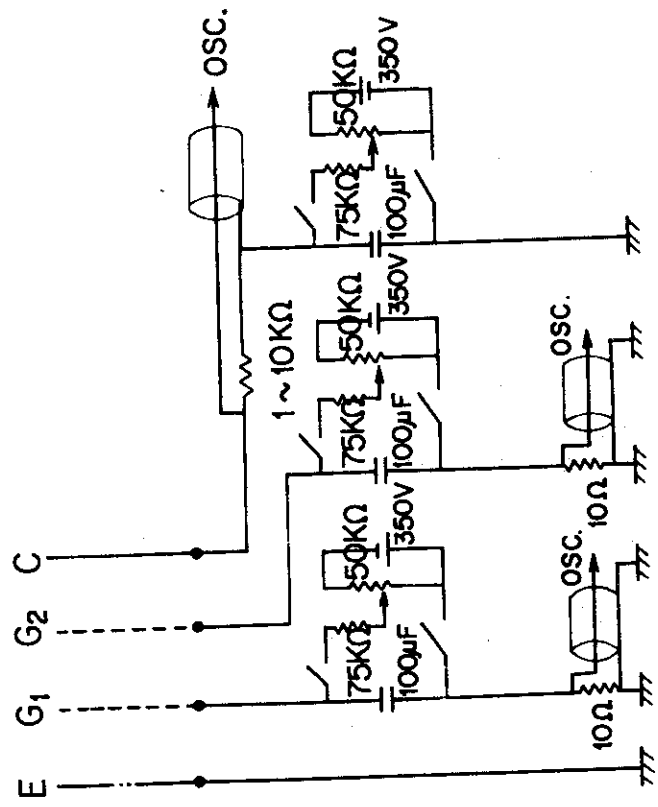

Fig. 2 Schematic drawing of an electrostatic multigrid energy analyzer and its circuit.

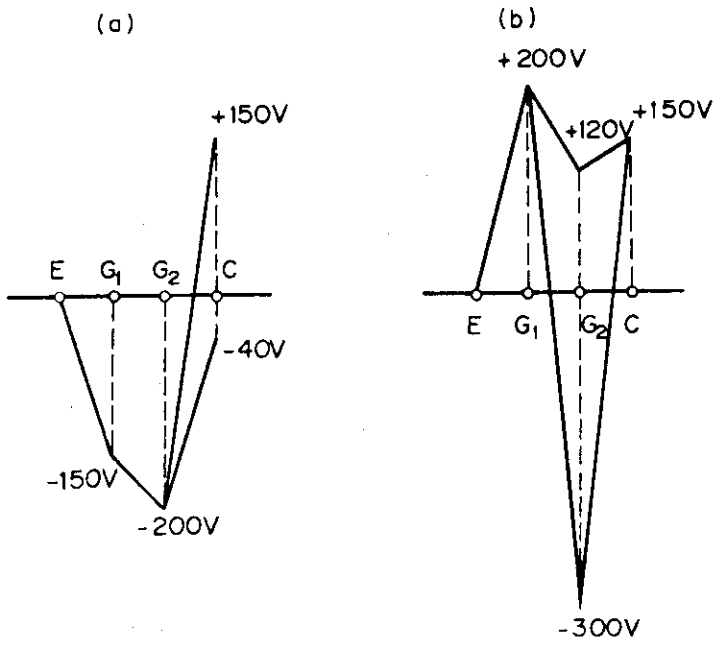

Fig. 3 Potential distribution between the grids E, G_1, G_2 and the collector C for (a) ion and (b) electron energy analysis.

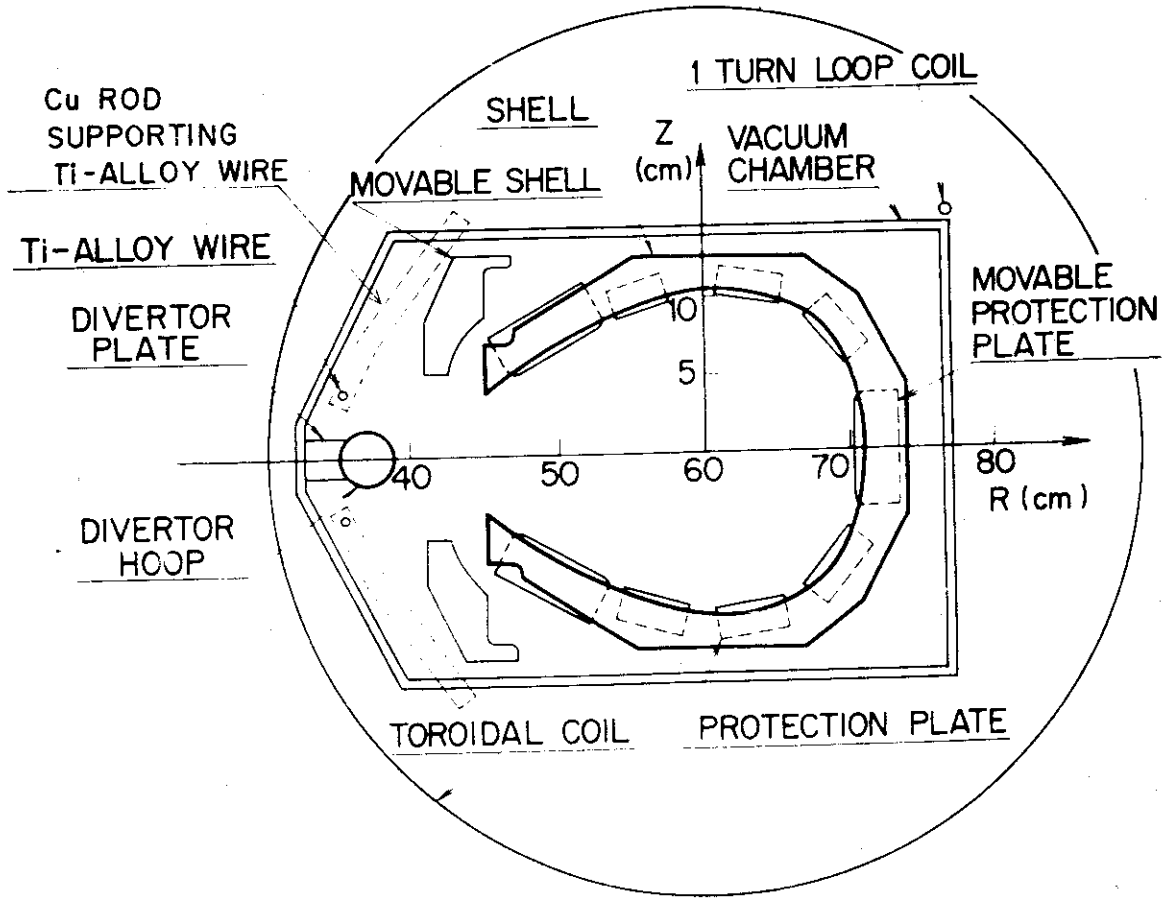

Fig. 4 Cross-sectional view of DIVA.

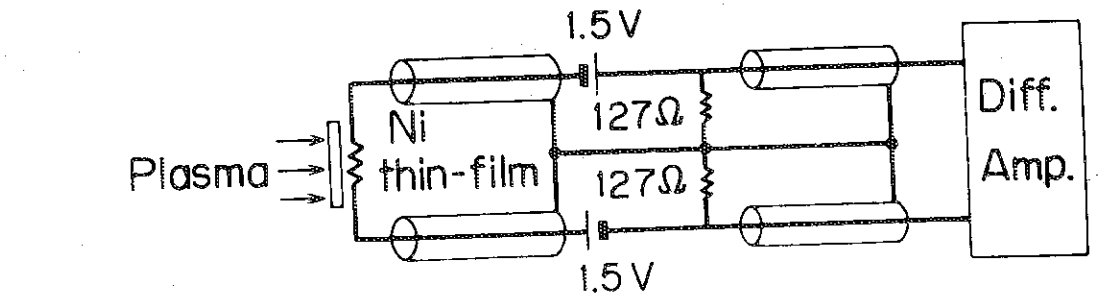

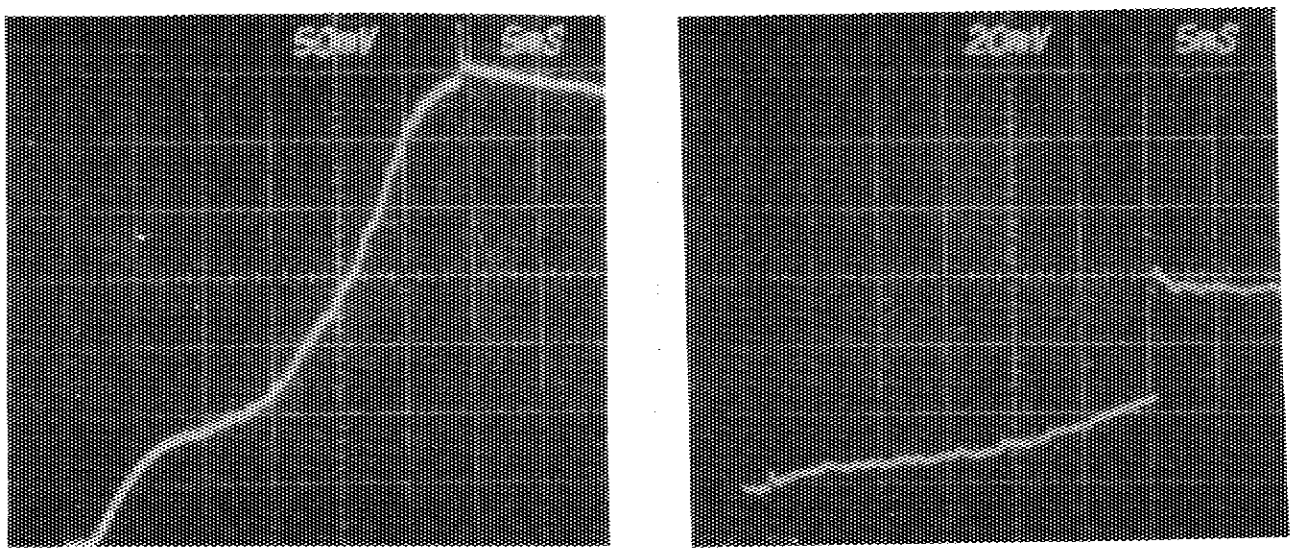

(a) R = 40 cm
Z = 4.5 cm

(b) R = 40 cm
Z = 3.0 cm

Fig. 5 Outputs of the thermometer located at different positions.

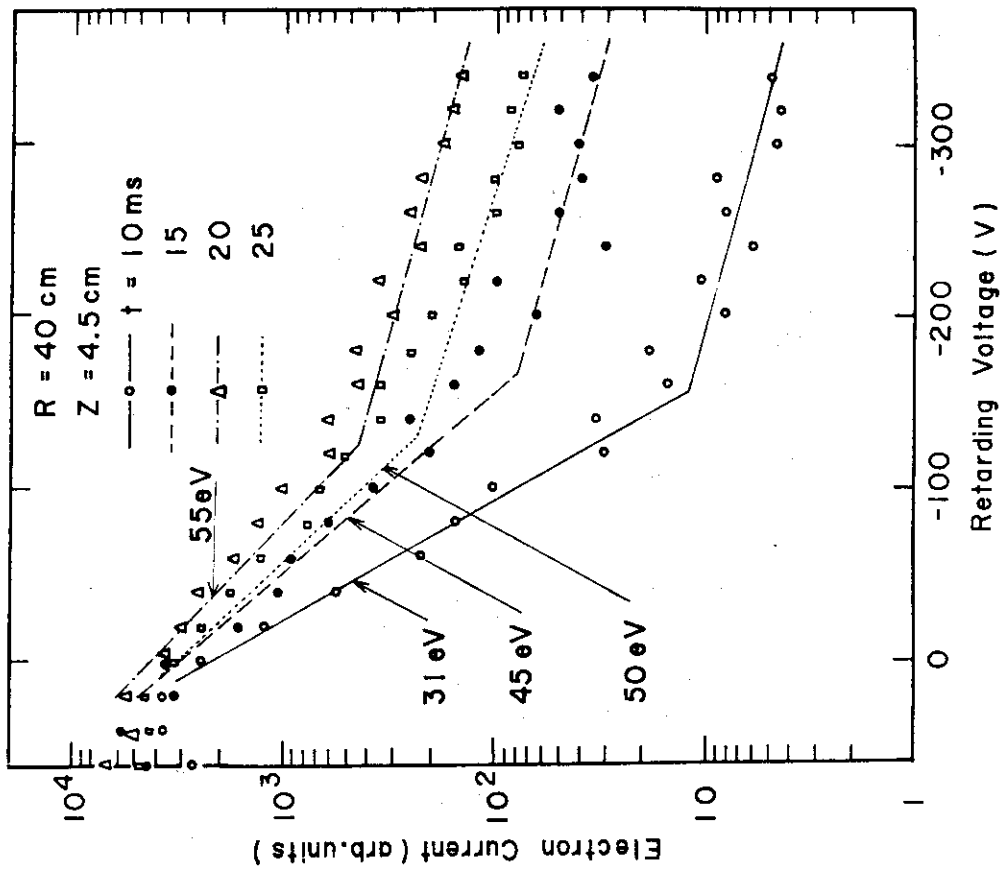

Fig. 7 Energy spectra of electrons in the electron side of divertor.

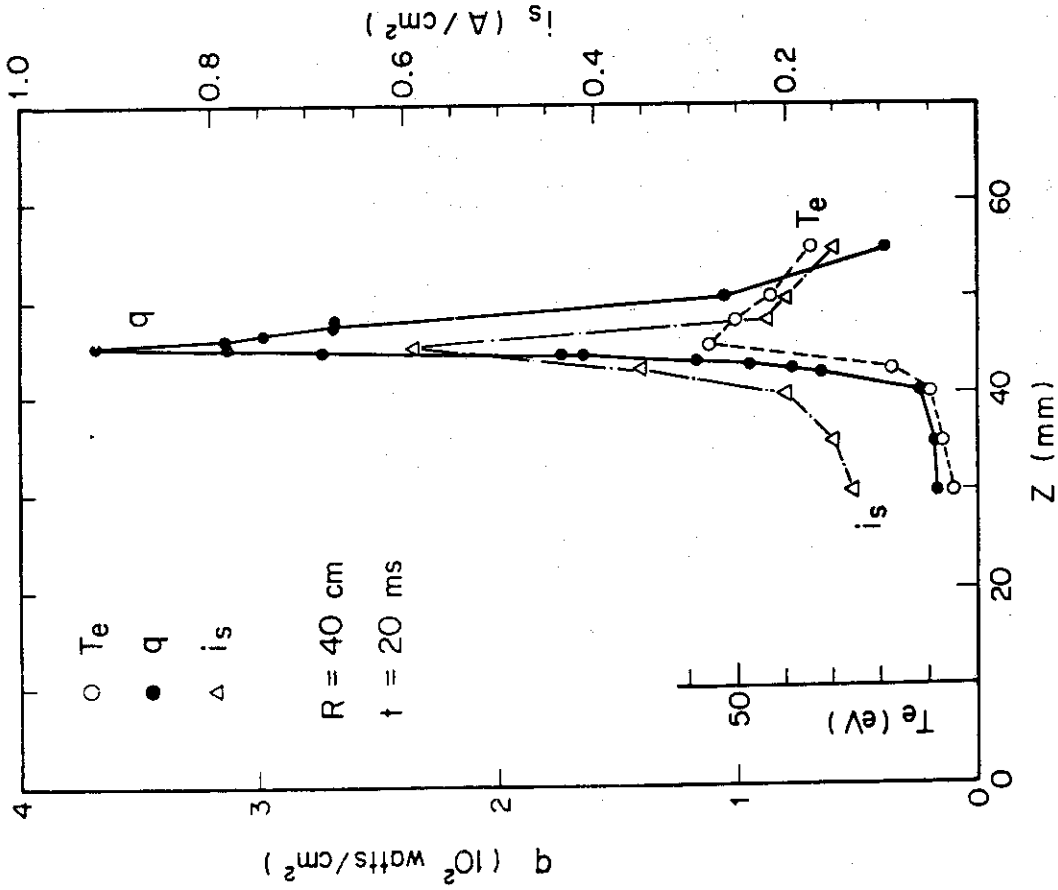

Fig. 6 Z-profiles of heat flux q, electron temperature T_e and ion saturation current density I_s in the electron side of divertor.

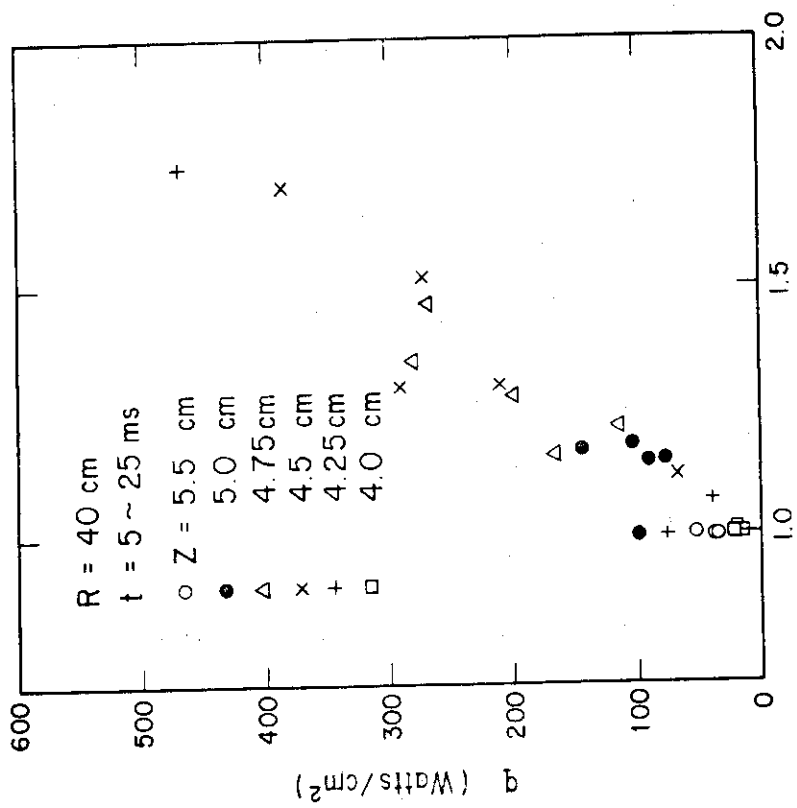

Fig. 9 Relationship between heat flux q and correction factor F for a two component model.

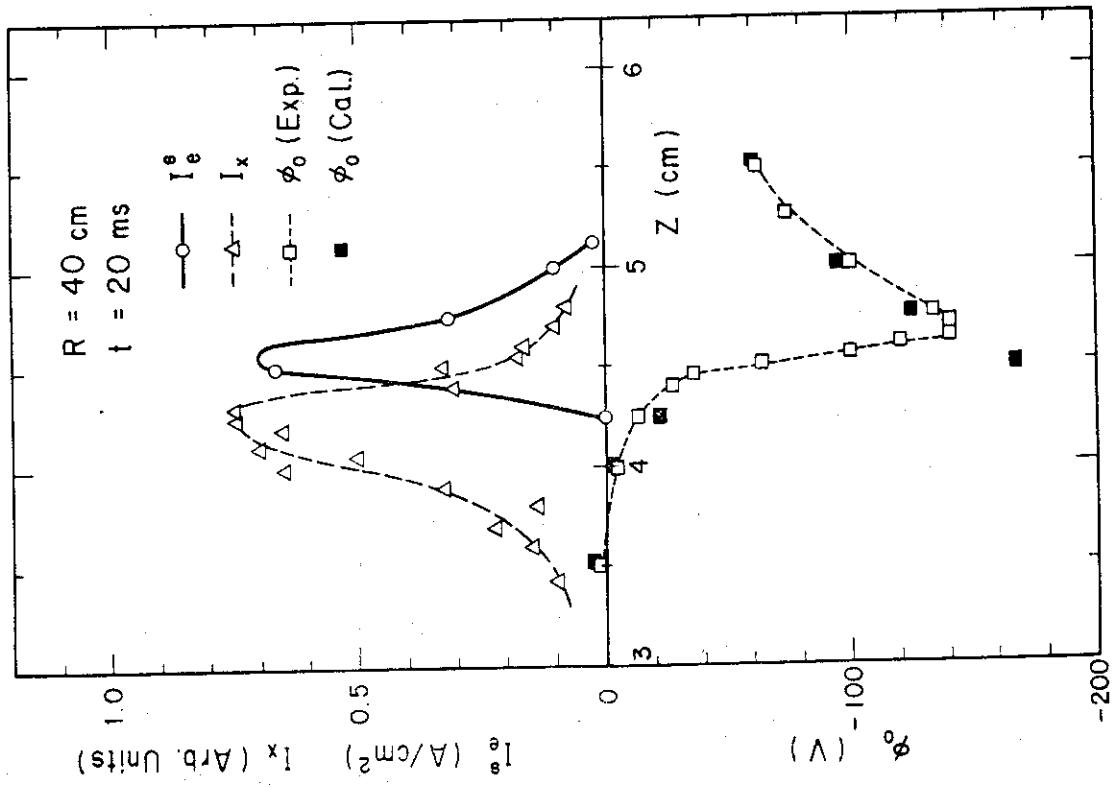

Fig. 8 Z-profiles of epithermal electron flux I_e^h, X-ray intensity I_x and floating potential ϕ_o in the electron side of divertor.

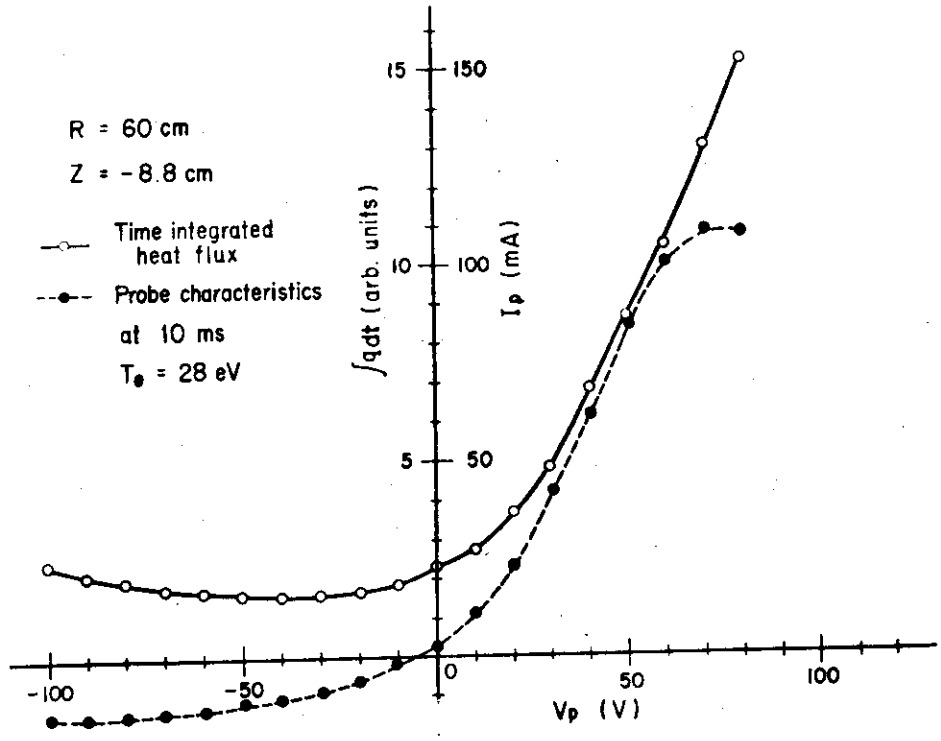

Fig.10 Time integrated heat flux in the whole discharge duration to a thermocoaxis as a function of a bias voltage V_p of a sheath of the thermocoaxis, together with a probe characteristic at 10 ms employing the sheath as an electrode.

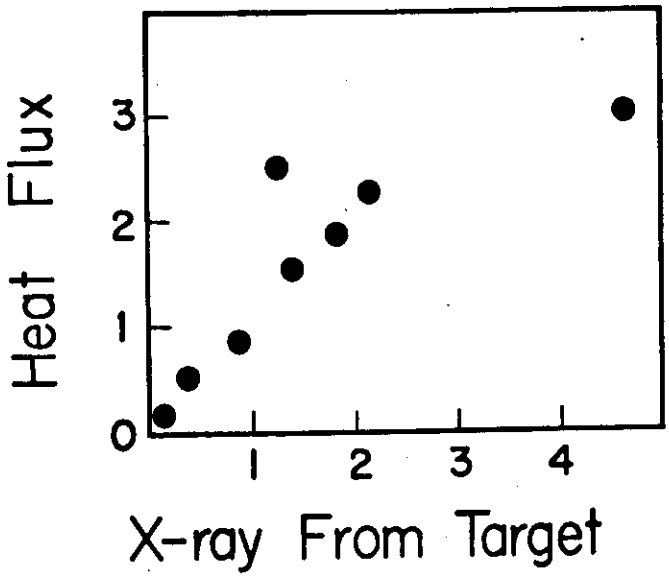

Fig.11 Correlation between time integrated heat flux and time integrated X-ray intensity from the target placed at the position of I_x peak with various discharges.